Copyright © 2008 Tech Science Press CMES, vol.33, no.1, pp.49-84, 2008

Dynamic Nonlinear Material Behaviour of Thin Shells in Finite Displacements and Rotations

C.E. Majorana[1] **and V.A. Salomoni**

Abstract: A dynamic analysis of a thin shell finite element undergoing large displacements and rotations is here presented. The constitutive model adopted derives from the coupling of an hyperelastic basic model fulfilling a De Saint Venant-Kirchhoff criterion with a scalar damage function depending on the maximum value of a suitable strain measure attained through the deformation history; then plastic effects are included using an isotropic/kinematic hardening law. A conservative time integration scheme for the non-linear dynamics of the hyperelastic damaged-plastic thin shell is applied. The main characteristic of the scheme is to be conservative, since it allows for the time-discrete system to preserve the basic laws of continuum, namely the balance of the linear and angular momentum as well as the fulfilment of the second law of thermodynamics.

Keyword: thin shells, large displacements and rotations, non-linear dynamics, time integration algorithms, hyperelastic-damage, plastic behaviour.

1 Introduction

The topic of nonlinear analysis of shells has been considered by many authors in recent years. Starting from classical solutions in elastostatic and elastodynamics, enhancements have been produced to include nonlinear geometry and inelasticity. Consequently, numerical algorithms have been adopted to resolve efficiently the complex nonlinear dynamics problems posed. As solution methods, popular FEM or BEM approaches have been accompanied by MLPG method. Within the latter solution strategy, [Sladek, Sladek, Wen and Aliabadi (2006)] found a solution of bending problems of shear deformable shallow shell starting from the Reissner theory. Static and dynamic loads were considered. Time-dependence was solved through Laplace transform technique. Weak formulation was adopted transforming the governing equations into local integral equations in the mean surface of the

[1] Department of Structural and Transportation Engineering, Faculty of Engineering, University of Padua, Italy.

shell. In that paper, nodal points are randomly spread on that surface and each integral is referred to a circular domain surrounding each node. Meshless approximation based on Moving Least-Squares (MLS) method allowed to solve the boundary integral equations generated. Comparison with FEM and BEM solutions are proposed, for circular and square shallow spherical shells showing good agreement specially between MLPG and FEM.

In another paper, [Baiz and Aliabadi, (2006)] considered the linear buckling problem of elastic shallow shells by a shear deformable shell theory. Boundary domain integral equation were obtained by coupling 2D plane stress elasticity with Reissner plate bending BEM formulation. Buckling problem was stated as standard eigenvalue problem. Boundary was discretized using quadratic isoparametric elements. Cylindrical shallow curved plates were studied with different dimensions and boundary conditions showing a good comparison with FEM results.

Again, MLPG method has been chosen by [Jarak, Soric and Hoster (2007)] to solve shell structure problems. 3D solid concept was employed incorporating 3D constitutive models, and exactly describing the shell geometry. Thickness locking has been eliminated through hierarchical quadratic functions along the thickness. Shear locking in thin structures was also minimized applying high order interpolation functions. Cylindrical shells (Scordelis-Lo shell roof) were considered as examples showing convergence properties of the method.

A geometrically nonlinear analysis of Reissner-Mindlin plates has been carried out by [Wen and Hon (2007)] using a meshless collocation method. Smooth radial basis functions (RBFs) allowed them to evaluate higher order derivatives at computational low costs. Coupled nonlinear terms in the governing equations were treated as body force for both plane stress and plate bending problems and results were compared with ABAQUS ones.

Finite rotation shell elements have been considered by [Kulikov and Plotnikova (2008)]. The authors described exactly the geometry and reference surface by analytically given functions and displacement vectors resolved in the reference surface frame. 3D constitutive equations have been used in the formulations. Six displacement of the outer surfaces and a transverse displacement of the midsurface allowed to derive strain-displacements relationships invariant under arbitrarily large ridigbody motions. Shear and membrane locking as well as spurious energy modes have been circumvented through assumed strain and stress resultant fields (ANS method). Incremental Total Lagrangian formulation allowed to resolve benchmark problems like cantilever curved beam under shear load, rectangular cross-ply plate and pinched emispherical and hyperbolic shell, showing that a coarse mesh can be adopted with extremely large displacements and rotations, insensitive to the number of load increments.

More recently, [Chui, Liu, Li, Zhao, Nguyen and Sun (2008)] introduced bilinear quadratic elements to resolve the geometrically nonlinear plate and shell problem posed. Elements have been divided into smoothing cells to perform strain smoothing operation. Three smoothing cells for bending strain energy and one smoothing cell for shear strain energy integration give accurate results. Total Lagrangian approach was adopted. Arc-length technique and modified Newton-Raphson method have been used to solve nonlinear equations. Square and circular plates have been investigated, as well as cylindrical panels as examples to show convergence properties and different boundary conditions effects. Then the practical application of the reinforcing plate of an automobile's front longeron has been also investigated.

Among elastoplastic solutions, [Tonkovic, Soric and Skozrit (2008)] analysed the case of cyclic elastoplastic deformation of shell structures, using an highly nonlinear multicomponent forms of kinematic and isotropic hardening functions within Von-Mises criterion, within a Reissner-Mindlin type formulation in tensor form. Consistent elastoplastic tangent modulus has been derived ensuring fast convergence rate and assumed strain isoparametric finite shell element allowed to capture finite rotations. Examples concerning spherical cap and cylindrical shallow shell under cyclic load, showed ratcheting effects and stabilization of load-displacement response for the proposed method of analysis.

Further developments have been published concerning the presence of internal support conditions in elastoplastic transient response of Reissner-Mindin plates [Providakis (2007)]; buckling and free vibration of shells [Sharnappa, Ganesan and Raju Sethuraman (2007)], while a Fourier series solution method has been proposed by [Suetake (2006)] always useful for reference purposes.

The contribution of the authors of this paper belong to the FEM family solution of thin shells. The mechanical description of the shell steams from an approach related to the standard formulation of the shell parametrization discussed in [Brank, Briseghella, Tonello, Damjanic (1998); Brank, Mamouri, Ibrahimbegovic (2005)]. The present approach is closed to these works especially as regards:

- the kinematics of the shell and, in particular, the description of the finite rotations and their updating in the discrete time system;
- the definition of the elastic constitutive model adopted as basis for the definition of the elasto-damage constitutive model;
- the general approach in the definition of the weak form, its discretization and linearization method.

On the other side, the method is modified regarding the choice of the constitutive model. This fact has some consequences in terms of:

- definition of internal forces and dissipation;
- method for the evaluation of the conservative algorithmic forms of dissipation;
- specific aspects in the application of the Newton method adopted for the linearization of the weak form.

The constitutive model adopted to include damage effects is chosen to have an internal dissipation in view of describing a real fragile/ductile material behaviour, as e.g. concrete under high stress states. These appears e.g. when concrete under high temperature is considered, approaching spalling behaviour, not yet satisfactory predictable with actual standard theories. Hence this approach can be considered a first step towards the above objective and has potentialities for practical industrial applications. The elastic-damage model here adopted is obtained starting from the definition of the De Saint Venant-Kirchhoff elastic model coupling the related stored energy function with a scalar damage function. The resulting constitutive model is similar to those proposed for the description of elastomeric materials, where the fraction of damage depends on the maximum value attained by an equivalent strain measure in the strain history of the material [Simo (1987)], but with changes in the parameters under tension and compression it can be well adapted for concrete, as e.g. in [Gawin, Majorana, Schrefler (1999); Salomoni, Mazzucco, Majorana (2007); Salomoni, Majorana, Giannuzzi, Miliozzi (2008)].

Plastic effects are included using strictly quadratic hyperelastic and hardening potentials, within an additive decomposition of the elastic and plastic deformations [Simo, Kennedy, Govinjee (1988)]. In some situations, unilateral contact of the deforming shell with rigid surfaces can appear, hence this feature has been also considered and included [Majorana, Bressanin, Rigo Serra, Zavarise (2002); Janna, Majorana, Zavarise (2004)]. Anyway, such aspects will be described in another paper.

The space discretization is made by using isoparametric four-node elements, in order to preserve the conservative character of the algorithm. Possible shear locking problems, arising in case of thin shells, are avoided through the adoption of the 'assumed natural strain' (ANS) approach [Dvorkin, Bathe (1984); Başar, Kintzel (2003)]. The weak form of the balance of momentum is linearized by using the Newton-Raphson method leading to a second order scheme. Some details on the calculation of the internal forces term of the weak form are given, together with the procedure adopted in order to get the algorithmic forms of stress and dissipation that lead to the conservative character of the time integration scheme.

An energy-momentum method is applied to the non-linear dynamics of thin shells,

made of materials with internal dissipation. The approach follows the method already applied to the elasto-damaged continuum dynamics in finite strains [Briseghella, Corazzin, Majorana, Pavan (1997); Briseghella, Majorana, Pavan (1998); Briseghella, Majorana, Pellegrino (1999); Briseghella, Majorana, Pavan (2000)] and to thin shells [Briseghella, Majorana, Pavan (2006)]. Further applications of the integrator concerns dynamic stability of beams and rods [Briseghella, Majorana, Pellegrino (1998); Majorana, Pellegrino (1999)]. The energy-momentum method is a time integration algorithm that has been formulated with respect to the rigid body [Simo, Wong (1991)], the continuum [Simo, Tarnow (1992)], the shells [Simo, Rifai (1992)] and rods dynamics [Simo, Tarnow, Doblare (1995)].

The subject of energy–momentum integration scheme in non-linear dynamics of shells has been also investigated in [Sansour, Wagner, Wriggers, Sansour (2002)]. In that paper the non-linear dynamics of shells using a model reformulated within the context of enhanced strain elements has been considered. In addition to the momentum and the angular momentum, the integration scheme also preserves the energy of a Hamiltonian system independent of the non-linearity involved in the strain–displacement relations. The enhanced strains have been treated as system parameters which are determined at any time step by a corresponding time-independent equation. Accordingly, the enhanced strains are not interpolated within a time step. The method has been also applied to shell instability under combined axial and transversal loadings.

Plastic behaviour in nonlinear shell analysis has been the objective of [Argyris, Papadrakakis, Karapitta (2002)]. The authors considered a layered elasto-plastic constitutive model based on the von Mises yield criterion with isotropic hardening within a geometrically nonlinear shell element, called TRIC. The characteristic feature of this element was that the nonlinear material behaviour is taken into account entirely on the natural coordinate system and can be expressed analytically for each layer. Then, the total natural tangent stiffness matrix is computed by adding together the tangent stiffness matrix of each layer. Both formulations based on the continuum and consistent elasto-plastic constitutive matrix are implemented. It was shown that the consistent elasto-plastic formulation performs the continuum one in both convergence behaviour and computational time, whereas the obtained results demonstrate, as in case of geometrically nonlinear analyses, that the TRIC shell element can treat geometric and material nonlinearities of arbitrary shells in an accurately and cost-effective way.

More recently, the performance of shell finite elements in finite strains has been discussed, as e.g. in [Areias, Song, Belytschko (2005)], where an improved 16 degrees-of-freedom quadrilateral shell element based on pointwise Kirchhoff–Love constraints was presented, introducing a consistent large strain formulation. The

model is based on classical shell kinematics combined with continuum constitutive laws of isotropic elastic type. The resulting element is valid for large rotations and displacements. The formulation is free of enhancements, it is almost fully integrated and is found to be immune to locking or unstable modes. No internal degrees-of-freedom are employed because of the simplicity of the constitutive law. From the practical viewpoint this constitutes a considerable advantage, as available continuum constitutive models can be employed without modification and the specific shell kinematics remove the need of accounting for the transverse shear energy (which, for large strain elasto-plasticity, is frequently assumed to be of elastic origin only). The performed finite element implementation is based on a four-node quadrilateral with 4 mid-side rotations and 3 displacement degrees-of-freedom per node. The generated element can be classified as a discrete Kirchhoff type one. Symmetric shape functions for the director field were developed and based on the model on classical Naghdi shell theory (neglecting the transverse shear energy terms). Five quadrature points were employed for each element, along two lines bisecting the parent domain, circumventing the difficulties previously associated with warped elements. The performance of the element in the tests in both linear and non-linear regimes was very good, when compared with other high performance elements available in literature, some of them making use of internal degrees-of-freedom. In particular, mesh distortion sensitivity was extremely low, since an elastic constitutive law was adopted.

Again, in the purely elastic field, a paper has been presented [Kulikov, Plotnikova (2006)] where the representation of arbitrarily large rigid-body motions in the displacement patterns of curved Timoshenko–Mindlin-type (TM) shell elements has been considered. This required the development of strain–displacement equations of the finite deformation TM shell theory, written in local curvilinear coordinates, with regards to their consistency with the large rigid-body motions. For this purpose the displacement vectors of the face surfaces are introduced and solved in the reference surface frame. In that paper economical schemes of evaluating the stiffness matrix by means of the analytical integration inside the element and an advanced approach for solving incremental equilibrium equations are discussed. The developed approach may allow for the use of very large load increments. The presented numerical results demonstrate the high accuracy and effectiveness of the developed four-node curved shell elements compared with performance of non-linear solid-shell elements extracted from literature. However, the limitation due to considered elastic behaviour should be remarked.

Going back to the energy-momentum method here considered, this algorithm is an implicit scheme, defined as conservative because it ensures the fulfillment of the basic laws of continuum, i.e. the balance laws of linear and angular momentum and

the balance of energy of the system. The conservation of the energy of the system leads to define the method as unconditionally stable. This means, for example, that for an elastic body subjected only to initial conditions (assigned configuration and velocity fields) and in absence of external loading, the total energy of the system, discretized in time, represents a constant of the motion, i.e. what happens in the continuum system. This property is not preserved by other types of integration schemes such those belonging to the Newmark's family if applied to non linear dynamics of elastic systems because the latter can ensure the balance of the linear and angular momentum only. Hence, this time integration scheme has been applied in particular to long term dynamics of elastic systems ensuring a similar description of the motion in contrast with solutions arising from other types of schemes.

The conservative character of the scheme, if applied to a system with internal dissipation, must be intended as the fulfilment of the Clausius-Duhem inequality in time in its discrete form. On the other side, for elastic systems the latter inequality leads simply to the equivalence between the rate of the stored energy function of the material and the internal power, i.e. the rate of work made by the internal forces.

In the final part of this paper, numerical examples are discussed showing the performance of the element when geometrical and material nonlinearities act simultaneously. The properties of the adopted time integration scheme in terms of fulfilment of the balance laws of the linear and angular momentum, as well as of the discrete form of the Clausius-Duhem inequality, are also shown, emphasizing the convergence characteristics.

2 Kinematics of shells

The reference configuration of the shell is defined by $\Omega \subseteq R^3$, the motion is the set of configurations given by $\varphi(\Omega,t) : R^3 \times [0,T] \rightarrow R^3$, where $[0,T]$ is the time interval of interest.

A point in the reference configuration of the shell is given by:

$$\bar{\mathbf{X}}\left(\xi^1,\xi^2,\xi\right) = \mathbf{X}\left(\xi^1,\xi^2\right) + \xi\mathbf{T} \tag{1}$$

where $\mathbf{X}$ is a point belonging to the mid-surface of the shell. The unit vector $\mathbf{T}$ is normal to the mid-surface at point $\mathbf{X}$.

The adopted system of coordinates ξ^1, ξ^2, ξ is defined with ξ^1, ξ^2 lying on the mid surface and ξ along $\mathbf{T}$. The variable ξ assumes the values $\xi \in [-h/2,+h/2]$, where h is the thickness of the shell. The points of the current, or deformed, configuration of the shell are defined by

$$\bar{\mathbf{x}}\left(\xi^1,\xi^2,\xi\right) = \mathbf{x}\left(\xi^1,\xi^2\right) + \xi\mathbf{t} \tag{2}$$

with **t** the unit vector. The unit vectors **T** and **t** are called the inextensible directors of the shell. A simple representation of the coordinate system in the reference configuration is shown in Figure 1.

The displacements of a generic point of the shell **U** and of a point belonging to its mid surface **u** are defined as

$$\mathbf{U} = \bar{\mathbf{x}} - \bar{\mathbf{X}}, \quad \mathbf{u} = \mathbf{x} - \mathbf{X} \tag{3}$$

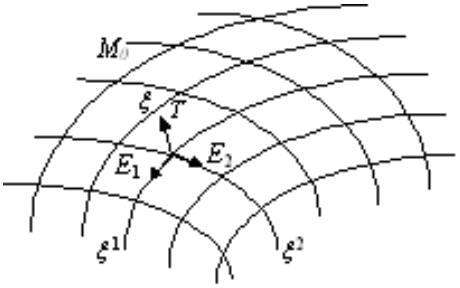

Figure 1: Reference system of coordinates of the shell mid plane.

Adopting a Lagrangian description [Suetake, Iura, Atluri (2003)] of the shell kinematics, the strains are described in terms of the Green-Lagrange tensor, defined by

$$\mathbf{E} = \frac{1}{2}\left(\mathbf{g}_i \cdot \mathbf{g}_j - \mathbf{G}_i \cdot \mathbf{G}_j\right)\mathbf{G}^i \otimes \mathbf{G}^j \qquad (i = 1,2,3) \tag{4}$$

The terms $\mathbf{G}_i$ and $\mathbf{g}_i$ are the covariant components, while $\mathbf{G}^i$ are the contravariant components (dual basis of $\mathbf{G}_i$) of the metric in the material and, respectively, the spatial reference systems. The covariant basis in the undeformed configuration is defined as

$$\mathbf{G}_\alpha = \partial\bar{\mathbf{X}}/\partial\xi^\alpha, \quad \mathbf{G}_3 = \partial\bar{\mathbf{X}}/\partial\xi \qquad (\alpha = 1,2) \tag{5}$$

while in the current reference systems one has

$$\mathbf{g}_\alpha = \partial\bar{\mathbf{x}}/\partial\xi^\alpha, \quad \mathbf{g}_3 = \partial\bar{\mathbf{x}}/\partial\xi \qquad (\alpha = 1,2) \tag{6}$$

According to the assumption made with the choice of the parametrization represented by Eq. (1) if the thickness h of the shell is small, the components of the Green-Lagrange strain tensor are such that

$$E_{ij} = E_{ij}^{(0)} + \xi E_{ij}^{(1)} + \xi^2 E_{ij}^{(2)} \quad (i = 1,2,3) \tag{7}$$

With the assumption of a thin shell, the terms of the second order in ξ can be neglected, while with relations (4), (5) and (6) at hands we obtain

$$E^{(0)}_{\alpha 3} = E^{(0)}_{3\alpha} = \frac{1}{2}\left[\partial \mathbf{X}/\partial \xi^{\alpha} \cdot (\mathbf{t}-\mathbf{T}) + \partial \mathbf{u}/\partial \xi^{\alpha} \cdot \mathbf{t}\right] \tag{8}$$

$$E^{(0)}_{\alpha\beta} = \frac{1}{2}\left[\partial \mathbf{X}/\partial \xi^{\alpha} \cdot \partial \mathbf{u}/\partial \xi^{\beta} + \partial \mathbf{X}/\partial \xi^{\alpha} \cdot \partial \mathbf{u}/\partial \xi^{\alpha} + \partial \mathbf{u}/\partial \xi^{\alpha} \cdot \partial \mathbf{u}/\partial \xi^{\beta}\right] \tag{9}$$

$$E^{(1)}_{\alpha\beta} = \frac{1}{2}\Big[\partial \mathbf{X}/\partial \xi^{\alpha} \cdot \partial\left(\mathbf{t}-\mathbf{T}\right)/\partial \xi^{\beta} + \partial \mathbf{X}/\partial \xi^{\beta} \cdot \partial\left(\mathbf{t}-\mathbf{T}\right)/\partial \xi^{\alpha} + \partial \mathbf{u}/\partial \xi^{\alpha} \cdot \partial \mathbf{t}/\partial \xi^{\beta} + \partial \mathbf{u}/\partial \xi^{\beta} \cdot \partial \mathbf{t}/\partial \xi^{\alpha}\Big] \tag{10}$$

Moreover, the component E_{33} vanishes. Further assumptions are introduced in order to simplify the formulation of the shell structure. The covariant and contravariant components in the reference configuration are approximated by their values in the mid plane of the shell M_0

$$\mathbf{A}_i = \mathbf{G}_i|_{\xi=0} \quad \mathbf{A}^i = \mathbf{G}^i\big|_{\xi=0} \quad (i = 1,2,3) \tag{11}$$

This makes possible to integrate the stress components through the thickness of the shell obtaining the stress resultants. All the details about the indicated procedure can be found in [Brank, Briseghella, Tonello, Damjanic (1998)]. The strain components can be identified as membrane, transverse shear and bending components

$$\varepsilon = \left[E^{(0)}_{11},\, E^{(0)}_{22},\, 2E^{(0)}_{12}\right]^T \tag{12}$$

$$\gamma = \left[2E^{(0)}_{13},\, E^{(0)}_{23}\right]^T \tag{13}$$

$$\kappa = \left[E^{(1)}_{11},\, E^{(1)}_{22},\, 2E^{(1)}_{12}\right]^T \tag{14}$$

The inextensible directors of the shell mid-surface in the reference and current configurations are related through an orthogonal tensor, element of the not-commutative space of rotations SO(3):

$$\mathbf{t} = \mathbf{R}\mathbf{T}, \quad \mathbf{R} \in SO(3) = \left\{\mathbf{R} \,:\, \mathbf{R}^T = \mathbf{R}^{-1}, \det \mathbf{R} = 1\right\} \tag{15}$$

Every orthogonal tensor represents a finite rotation around a vector $\mathbf{s}$ (the axis of rotation). A skew-symmetric tensor $\mathbf{S}$

$$\mathbf{S} \in so(3) = \left\{\mathbf{S} :\, \mathbf{S}^T = -\mathbf{S}\right\} \tag{16}$$

can be associated to the vector **s** (which is called axial of **S**). The set $so(3)$ is the space of infinitesimal rotations. The skew-symmetric tensor **S** is defined by the properties $\mathbf{Ss} = \mathbf{0}$ and $\mathbf{Sb} = \mathbf{s} \times \mathbf{b}$, fulfilled by any vector **b**. The tensors **S** give the rotation tensor **R** through the exponential map

$$\mathbf{R} = \exp[\mathbf{S}] = \mathbf{I} + (\sin \|\mathbf{s}\|/\|\mathbf{s}\|)\mathbf{S} + \left[(1 - \cos \|\mathbf{s}\|)/\|\mathbf{s}\|^2\right]\mathbf{S}^2 \tag{17}$$

The main characteristic of the representation of **R** tensor through the exponential map (called also Rodrigues' formula) is to result free from any singularity. This is particularly important if the system to be described undergoes large rotations (as the case here considered). The velocity of a point of the shell mid-plane (derivative with respect to time of **x**) will be indicated by $\dot{\mathbf{x}}$ and the angular velocity of the director t will result $\omega = \mathbf{t} \times \dot{\mathbf{t}}$.

3 Constitutive model

The choice of the constitutive model is here motivated to obtain a material with internal dissipation. The definition of an elastic-damage model such as the one here presented has the advantage to lead to simple expressions of the internal forces as well as of the terms arising from the linearization of the weak form. The elastic-damage constitutive model is defined starting from the elastic De Saint Venant-Kirchhoff constitutive model. The stored energy function is coupled in multiplicative way with a scalar damage function defining the Helmholtz free-energy function.

3.1 Hyperelastic constitutive model

For the hyperelastic De Saint Venant-Kirchhoff constitutive model, the relation between the second Piola-Kirchhoff stress tensor and the Green-Lagrange strain tensor is given by

$$\mathbf{S} = \mathbf{H} : \mathbf{E} = \lambda tr[\mathbf{E}]\mathbf{I} + 2\mu\mathbf{E} \tag{18}$$

where λ and μ are the Lamè's elastic constants. In terms of components one has

$$H^{ijkl} = \lambda G^{ij} G^{kl} + \mu \left(G^{ik} G^{jl} + G^{il} G^{jk}\right) \tag{19}$$

Following the standard procedure for the case of thin shell, the stress component along the normal direction to the mid plane of the shell itself is assumed to be zero and a reduced material tensor can be deduced from Eq. (19)

$$C^{ijkl} = H^{ijkl} - \frac{H^{33kl}}{H^{3333}} \quad (ij \neq 33,\ kl \neq 33) \tag{20}$$

According to the approximation assumed for the components of the metric, the terms of the reduced four rank tensor (20) are constant through the thickness of the shell, thus the membrane, transverse shear and bending resultant stresses are defined as

$$\mathbf{n} = n^{\alpha\beta}\mathbf{A}_\alpha \otimes \mathbf{A}_\beta \tag{21}$$

$$\mathbf{q} = n^{\alpha 3}\mathbf{A}_\alpha \otimes \mathbf{T} + n^{3\alpha}\mathbf{T} \otimes \mathbf{A}_3 \tag{22}$$

$$\mathbf{m} = m^{\alpha\beta}\mathbf{A}_\alpha \otimes \mathbf{A}_\beta \tag{23}$$

where the scalar components are given by

$$n^{ij} = \int_{-H/2}^{+H/2} C^{ijkl} E_{kl}^{(0)} d\xi, \quad ij \neq 33\,, \quad kl \neq 33 \tag{24}$$

$$m^{\alpha\beta} = \int_{-H/2}^{+H/2} C^{\alpha\beta\gamma\delta} E_{\gamma\delta}^{(1)} (\xi)^2 d\xi \tag{25}$$

On the basis of the assumed simplifications, the stored energy function associated to the constitutive relation (18) results in the sum of three terms related to the membrane, transverse shear and bending components of the strain respectively, which are not coupled. Adopting a matrix notation, the vector of the stress resultants $\mathbf{r}^T = \left[\mathbf{n}^T,\, \mathbf{q}^T,\, \mathbf{m}^T\right]$ can be deduced from

$$\mathbf{r} = \frac{\partial W(\Gamma)}{\partial \Gamma} \tag{26}$$

where the stored energy function is a quadratic form of the strain vector $\Gamma^T = \left[\varepsilon^T,\, \gamma^T,\, \kappa^T\right]$

$$W(\Gamma) = \frac{1}{2}\Gamma^T \begin{bmatrix} C^n & 0 & 0 \\ 0 & C^q & 0 \\ 0 & 0 & C^m \end{bmatrix} \Gamma \tag{27}$$

Additional details about the terms of the above matrix are given in the Appendix.

3.2 Elastic-damaged constitutive model

Starting from the elastic model defined in the previous section, in particular with the stored energy function (27) at hand, the Helmholtz free energy function can be defined as

$$\Psi = g(\Xi)\, W(\Gamma) \tag{28}$$

where g is a not-growing damage function and W is the stored energy function of an undamaged material. The g function can be defined, for example, by

$$g(\Xi) = b + a(1-b)\left(1 - e^{-\Xi/a}\right)/\Xi \tag{29}$$

where the constants a, b can assume the values $a \in]\,0, +\infty)$ and $b \in [0,1]$, respectively. For a zero value of Ξ the g function is equal to one (undamaged material). For increasing values of Ξ the g function is decreasing to the limit value of b if $\Xi \to \infty$. Hence the parameter b is related to the maximum damage, while a affects the rate of the damage growing with Ξ. In the formulation here assumed the variable Ξ represents an equivalent strain measure, based on the value of the stored energy function W of the material supposed undamaged. The equivalent strain is defined as the maximum value attained in the strain history of the material:

$$\Xi = \max_{\tau \in (-\infty, t]} \sqrt{2W(\Gamma(\tau))} \tag{30}$$

The Clausius-Duhem inequality

$$-\dot{\Psi} + \mathbf{r}^T \Gamma = D_{int} > 0 \tag{31}$$

on the basis of the free energy function assumed, leads to the expressions of the generalised stress resultants (components of the vector $\mathbf{r}$)

$$\begin{aligned} \mathbf{n} &= g(\Xi)\, C^n \varepsilon \\ \mathbf{q} &= g(\Xi)\, C^q \gamma \\ \mathbf{m} &= g(\Xi)\, C^m \kappa \end{aligned} \tag{32}$$

and of the internal dissipation

$$D_{int} = \frac{W(\Gamma)}{\Xi} \frac{dg(\Xi)}{d\Xi} \left[\frac{\partial W}{\partial \Gamma}\right]^T \dot{\Gamma} \geq 0. \tag{33}$$

The internal dissipation results not negative because of the assumption of a not growing damage function g. It is possible to define a damage surface by means of the equation

$$\phi(\Gamma, \Xi) = \sqrt{2W(\Gamma)} - \Xi = 0 \tag{34}$$

The surface ϕ gives the admissible values of the variables Γ and Ξ which must satisfy the following inequality

$$\phi(\Gamma, \Xi) \leq 0 \tag{35}$$

The previous inequality represents the damage criterion that can be re-assumed by the set of relations

$$\begin{cases} \dot{g}(\Xi) < 0 & \text{for } \phi = 0 \text{ and } [\partial\phi/\partial\Gamma]^T \dot{\Gamma} > 0 \\ \dot{g}(\Xi) = 0 & \text{otherwise} \end{cases} \tag{36}$$

The set of relations (36) means that the growing of damage occurs for a loading path starting from the damage surface.

3.3 Elastic-plastic constitutive model

For the elastic-plastic constitutive model, strictly quadratic hyperelastic and hardening potentials are chosen, using an additive decomposition of the elastic and plastic deformations:

$$\mathbf{W}(\varepsilon - \varepsilon^p) := \frac{1}{2}(\varepsilon - \varepsilon^p)^t C(\varepsilon - \varepsilon^p) \Rightarrow \sigma = \nabla\mathbf{W}(\varepsilon - \varepsilon^p) = C(\varepsilon - \varepsilon^p), \quad \sigma, \varepsilon \in R^8 \tag{37}$$

$$H(\alpha) = \frac{1}{2}\alpha^t \mathbf{D}\alpha \Rightarrow \mathbf{p} = -\nabla H(\alpha) = -\mathbf{D}\alpha = -\begin{Bmatrix} D\alpha \\ \bar{\mathbf{D}}\bar{\alpha} \end{Bmatrix}, \quad \alpha, \mathbf{p} \in R^9 \tag{38}$$

Isotropic and kinematic hardening are included in the model, with 8 variables for the kinematic hardening and 1 for the isotropic one. It has been used the principle of maximum plastic dissipation, in the hypothesis of associative plasticity and hardening, which implied the use of symmetric iteration matrices, with considerable computational savings:

$$\dot{\varepsilon}^p = \sum_{\mu=1}^{n} \dot{\gamma}_\mu \partial_{\boldsymbol{\sigma}} \phi_\mu(\boldsymbol{\sigma}, \mathbf{p}) \qquad \text{and} \qquad \dot{\boldsymbol{\alpha}} = \sum_{\mu=1}^{n} \dot{\gamma}_\mu \partial_{\mathbf{p}} \phi_\mu(\boldsymbol{\sigma}, \mathbf{p}) \tag{39}$$

The chosen plastic surface is the Ilyushin-Shapiro one; it is a plastic surface directly formulated in terms of stress resultants, giving also a good approximation of the Von-Mises criterion. A term including the effect of the shear stress resultant has been added to the traditional relationship representing this surface. In matrix notation

$$\phi_\mu(\sigma,\mathbf{p}) \equiv (\sigma+\bar{\mathbf{p}})^t \mathbf{A}_\mu (\sigma+\bar{\mathbf{p}}) - \frac{(k_0+k'p)^2}{k_0^2} \leq 0, \quad \mu \in (1,2) \tag{40}$$

$$A_\mu = \begin{bmatrix} \frac{1}{n_0^2}\mathbf{P} & \mathbf{0} & \frac{sign(\mu)}{2\sqrt{3}n_0 m_0}\mathbf{P} \\ \mathbf{0} & \frac{1}{q_0^2}\mathbf{I}_2 & \mathbf{0} \\ \frac{sign(\mu)}{2\sqrt{3}n_0 m_0}\mathbf{P} & \mathbf{0} & \frac{1}{m_0^2}\mathbf{P} \end{bmatrix}, \qquad sign(\mu) := \begin{cases} +1 & \text{if } \mu = 1 \\ -1 & \text{if } \mu = 2 \end{cases} \tag{41}$$

In the above relationship $\{n_0, q_0, m_0\}$ represents the plastic threshold of the element in different loading conditions, i.e. uniaxial traction, pure shear and cylindrical bending. The coupling term between membrane and bending resultants generates a double plastic surface, since an absolute value function must be taken into account.

Consequently, a return mapping procedure able to manage double surfaces has been implemented, with two unknown shear deformations γ_1 and γ_2, corresponding to the cases with coupling term (between membrane and bending stress resultants) positive or negative, respectively.

Obviously, the stress state is limited by the Kuhn-Tucker conditions

$$\gamma_\mu \geq 0, \quad \phi_\mu \leq 0, \quad \gamma_\mu \phi_\mu = 0 \quad \mu \in (1,2) \tag{42}$$

Using the relationships employed for hardening plasticity and passing to the discrete form ($\gamma_1, \gamma_2 \Rightarrow \gamma_1^\kappa + \Delta\gamma_1^\kappa, \gamma_2^\kappa + \Delta\gamma_2^\kappa$), the plastic surface is reduced to depend on the unknown shear deformations only

$$\phi_\mu(\sigma,\mathbf{p}) \equiv \phi_\mu(\gamma_1^\kappa,\gamma_2^\kappa) = f_\mu(\gamma_1^\kappa,\gamma_2^\kappa) - \frac{[k(\gamma_1^\kappa,\gamma_2^\kappa)]^2}{k_0^2} \leq 0, \quad \mu \in (1,2) \tag{43}$$

The found relationship generates a nonlinear system of order 2, which must be appropriately solved. The chosen procedure is a Newton-Raphson cycle, with a relatively expensive linearization of expression (43), since square roots appears too, but exact and hence characterized by a quadratic convergence.

At each Newton iteration (we are talking about the local Newton cycle and not to the global one used for the whole system), a check on the Kuhn-Tucker conditions is performed and, if they are not fulfilled by at least one of the two shear strains ($\gamma_\mu^k > 0$), the corresponding surface is immediately deactivated. This procedure

implies that, even if the plastic surface is doubled, the most part of the operations are currently carried out on the active surface only, with noteworthy computational savings.

Also in this case the relation of the tangent algorithmic modulus has been found (including the isotropic/kinematic hardening), that in matrix notation appears as follows

$$\left[\frac{d\sigma}{d\varepsilon}\right]_{n+1} = \left[\overline{\mathbf{E}}_{\sigma,n+1}\right] - \left[\sum_{\alpha\in\mathbf{J}_{\text{act}}}\sum_{\beta\in\mathbf{J}_{\text{act}}} g^{\alpha\beta}\mathbf{N}_\alpha\mathbf{N}_\beta^t\right] \tag{44}$$

where

$$\begin{aligned}\left[\overline{\mathbf{E}}_{n+1}\right] = \left[\mathbf{E}_{n+1}\right]^{-1} = \begin{bmatrix}\mathbf{E}_{\sigma,n+1} & \mathbf{E}_{\sigma\bar{\mathbf{p}},n+1}\\ \mathbf{E}_{\sigma\bar{\mathbf{p}},n+1} & \mathbf{E}_{\bar{\mathbf{p}},n+1}\end{bmatrix}^{-1} &= \begin{bmatrix}\overline{\mathbf{E}}_{\sigma,n+1} & \overline{\mathbf{E}}_{\sigma\bar{\mathbf{p}},n+1}\\ \overline{\mathbf{E}}_{\bar{\mathbf{p}}\sigma,n+1} & \overline{\mathbf{E}}_{\bar{\mathbf{p}},n+1}\end{bmatrix}\\ &= \begin{bmatrix}\overline{\mathbf{E}}_{\sigma,n+1} & \overline{\mathbf{E}}_{\sigma\bar{\mathbf{p}},n+1}\\ \overline{\mathbf{E}}^t_{\sigma\bar{\mathbf{p}},n+1} & \overline{\mathbf{E}}_{\bar{\mathbf{p}},n+1}\end{bmatrix}_{16\times 16}\end{aligned} \tag{45}$$

with

$$\begin{aligned}\left[\mathbf{E}_{n+1}\right] &= \begin{bmatrix}\mathbf{E}_{\sigma,n+1} & \mathbf{E}_{\sigma\bar{\mathbf{p}},n+1}\\ \mathbf{E}_{\sigma\bar{\mathbf{p}},n+1} & \mathbf{E}_{\bar{\mathbf{p}},n+1}\end{bmatrix}\\ &= \begin{bmatrix}\left[C^{-1} + \sum_{\alpha\in\mathbf{J}_{\text{act}}}\gamma_\alpha^{n+1}\partial^2_{\sigma\sigma}\phi_\alpha\right] & \left[\sum_{\alpha\in\mathbf{J}_{\text{act}}}\gamma_\alpha^{n+1}\partial^2_{\sigma\sigma}\phi_\alpha\right]\\ \left[\sum_{\alpha\in\mathbf{J}_{\text{act}}}\gamma_\alpha^{n+1}\partial^2_{\sigma\sigma}\phi_\alpha\right] & \left[\overline{\mathbf{D}}^{-1} + \sum_{\alpha\in\mathbf{J}_{\text{act}}}\gamma_\alpha^{n+1}\partial^2_{\sigma\sigma}\phi_\alpha\right]\end{bmatrix}_{16\times 16}\end{aligned} \tag{46}$$

$$\mathbf{N}_\beta = \left[\overline{\mathbf{E}}^t_{\sigma,n+1} + \overline{\mathbf{E}}^t_{\sigma\bar{\mathbf{p}},n+1}{}^t\right]\left\{\partial_\sigma\phi_\beta\right\} = \left[\overline{\mathbf{E}}_{\sigma,n+1} + \overline{\mathbf{E}}_{\sigma\bar{\mathbf{p}},n+1}\right]\left\{\partial_\sigma\phi_\beta\right\} \tag{47}$$

$$g^{\alpha\beta} = \left[h_{\beta\alpha}\right]^{-1} \tag{48}$$

where

$$h_{\beta\alpha} = \left\{\partial_\sigma\phi^t_\beta,\quad \partial_\sigma\phi^t_\beta\right\}\left[\overline{\mathbf{E}}_{n+1}\right]\begin{Bmatrix}\partial_\sigma\phi_\alpha\\ \partial_\sigma\phi_\alpha\end{Bmatrix} + \partial_p\phi_\beta E_{p,n+1}\partial_p\phi_\alpha \tag{49}$$

and

$$E_{p,n+1} = \left[D^{-1} + \sum_{\alpha\in\mathbf{J}_{\text{act}}}\gamma_\alpha^{n+1}\partial^2_{pp}\phi_\alpha\right]^{-1} \tag{50}$$

Even if the relationships of the tangent modulus are relatively complex and heavy to be calculated, its use leads to a quadratic convergence speed of the full Newton-Raphson iteration cycle in the global system. Moreover, the above expression incorporates the Kuhn-Tucker conditions and this leads again to beneficial effects in terms of number of needed iterations to obtain convergence.

4 Balance equations

The following relation gives the total linear momentum of the system

$$\mathbf{L}\left(\dot{\Phi}\right)=\int_{\Omega}\rho_0\left(\dot{\mathbf{x}}+\xi\dot{\mathbf{t}}\right)d\Omega \tag{51}$$

where ρ_0 is the density in the reference configuration and the symbol Φ is used to indicate an element of the phase space represented by the pairs $(\mathbf{x},\mathbf{t})$. Integration through the thickness of the shell enables one to rewrite the equation (51) as

$$\mathbf{L}\left(\dot{\Phi}\right)=\int_{M_0}\mathbf{p}dM_0 \tag{52}$$

where the vector $\mathbf{p}$ is the linear momentum of the mid surface of the shell resulting from

$$\mathbf{p}=\rho_0 H\dot{\mathbf{x}} \tag{53}$$

Using a similar procedure, the total angular momentum of the shell

$$\mathbf{J}\left(\dot{\Phi},\Phi\right)=\int_{\Omega}\rho_0\left(\mathbf{x}+\xi\mathbf{t}\right)\times\left(\dot{\mathbf{x}}+\xi\dot{\mathbf{t}}\right)d\Omega \tag{54}$$

is obtained in the alternative form

$$\mathbf{J}\left(\dot{\Phi},\Phi\right)=\int_{M_0}\left(\mathbf{x}\times\mathbf{p}+\mathbf{t}\times\pi\right)dM_0 \tag{55}$$

The vector π is called director momentum. A comparison of the previous equations gives

$$\pi=\rho_0\frac{H^3}{12}\dot{\mathbf{t}} \tag{56}$$

Finally the kinetic and internal energy of the system are given by

$$K\left(\dot{\Phi}\right)=\frac{1}{2}\int_{M_0}\left(\rho_0 H\dot{\mathbf{x}}\cdot\dot{\mathbf{x}}+\rho_0\frac{H^3}{12}\dot{\mathbf{t}}\cdot\dot{\mathbf{t}}\right)dM_0 \tag{57}$$

$$V_{int}=\int_{M_0}g\left(\Xi\right)W\left(\Gamma\right)dM_0 \tag{58}$$

The basic laws of the continuum for a pure initial value problem, i.e. if the absence of external loading is supposed, are the conservation of the total linear momentum $\mathbf{L}$ and the total angular momentum $\mathbf{J}$ of the system

$$d\mathbf{L}\left(\dot{\Phi}\right)/dt = \mathbf{0} \quad d\mathbf{J}\left(\dot{\Phi},\Phi\right)/dt = \mathbf{0} \tag{59}$$

In addition, the balance of energy must fulfil the following inequality

$$d\left[K\left(\dot{\Phi}\right) + V_{int}\left(\Phi\right)\right]/dt = D_{int} \geq 0 \tag{60}$$

If the presence of a conservative loading is admitted, the related term of potential must be included in the previous inequality

$$\frac{d}{dt}\left[K\left(\dot{\Phi}\right) + V_{int}\left(\Phi\right) + V_{est}\left(\Phi\right)\right] = D_{int} \geq 0 \tag{61}$$

The weak form of the balance of momentum of the shell can be written as

$$G_{dyn}\left(\dot{\Phi},\Phi,\delta\Phi\right) = G_{ine}\left(\dot{\Phi},\delta\Phi\right) + G_{stat}\left(\Phi,\delta\Phi\right) - G_{ext}\left(\delta\Phi\right) \tag{62}$$

in which the terms relating to the inertial forces, to the internal forces and to the external loading are given respectively by

$$G_{ine}\left(\dot{\Phi},\delta\Phi\right) = \int_{M_0} (\dot{\mathbf{p}}\cdot\delta\mathbf{u} + \dot{\pi}\cdot\delta\mathbf{t})dM_0 \tag{63}$$

$$G_{stat}\left(\Phi,\delta\Phi\right) = \int_{M_0} (\mathbf{n}:\delta\varepsilon + \mathbf{q}:\delta\gamma + \mathbf{m}:\delta\kappa)dM_0 \tag{64}$$

$$G_{ext}\left(\delta\Phi\right) = -V_{ext}\left(\delta\Phi\right) \tag{65}$$

Equation (62) is completed by the initial conditions imposed on Φ

$$(\mathbf{x},\mathbf{t})|_{t=0} = (\mathbf{X},\mathbf{T}) \qquad (\mathbf{p},\pi)|_{t=0} = (\mathbf{p}_0,\pi_0) \tag{66}$$

The admissible variation of the elements of the phase space is obtained as directional derivative of Φ. The variations $\delta\mathbf{t}$ are tangent to the mid plane of the shell. Because of the inextensible character of $\mathbf{t}$, its variation satisfies the properties $\delta\mathbf{t}\cdot\mathbf{t} = 0$, resulting tangent to the unit sphere defined by $\mathbf{t}$ itself.

The substitution in the weak form of particular test functions makes possible to obtain the basic laws of balance represented by Eqs. (59), (60) and (61). It is expected that a finite element formulation arising from the discretization in time and space of the weak form let the balance laws to be fulfilled. This is what results from the procedure partially explained in the next sections.

5 Time integration scheme

In the present section some details about the application of the time integration scheme are presented. The total time interval of interest is divided in sub-intervals

$$[0,T] = \bigcup_{n=0}^{N} [t_n, t_{n+1}] \tag{67}$$

Let the configuration (displacement and velocity fields) of the system at time t_n be known. The problem of the integration in time is the evaluation of the unknown system configuration at time t_{n+1}. The displacement and velocity values in a generic intermediate time step of the interval $[t_n, t_{n+1}]$ is given as a linear combination of the values at the time instants t_n and t_{n+1}. The mid time configuration can be written as

$$(\mathbf{x},\mathbf{t})_{n+1/2} = \frac{1}{2}\left[(\mathbf{x},\mathbf{t})_n + (\mathbf{x},\mathbf{t})_{n+1}\right] \tag{68}$$

$$(\mathbf{p},\pi)_{n+1/2} = \frac{1}{2}\left[(\mathbf{p},\pi)_n + (\mathbf{p},\pi)_{n+1}\right] \tag{69}$$

By defining the amplitude of the generic time step $\Delta t = t_{n+1} - t_n$, the components of (69) are given as follows

$$\mathbf{p}_{n+1/2} = A_{\rho_0} \frac{\mathbf{x}_{n+1} - \mathbf{x}_n}{\Delta t} \tag{70}$$

$$\pi_{n+1/2} = I_{\rho_0} \frac{\mathbf{t}_{n+1} - \mathbf{t}_n}{\Delta t} \tag{71}$$

With the equations (70) and (71) at hand, the weak form of the balance can be discretized in time and evaluated in the mid-configuration of the time step

$$\frac{1}{\Delta t}\int_{M_0} \left[\delta\mathbf{u}\cdot(\mathbf{p}_{n+1} - \mathbf{p}_n) + \delta\mathbf{t}\cdot(\pi_{n+1} - \pi_n)\right] dM_0 + G_{stat}\left(\Phi_{n+1/2}, \delta\Phi\right) - G_{est}\left(\delta\Phi\right) = 0 \tag{72}$$

The previous relation is obtained by using the following expressions of the rate of $\mathbf{p}$ and π in the mid-configuration

$$\dot{\mathbf{p}}_{n+1/2} = \frac{\mathbf{p}_{n+1} - \mathbf{p}_n}{\Delta t} \tag{73}$$

$$\dot{\pi}_{n+1/2} = \frac{\pi_{n+1} - \pi_n}{\Delta t} \tag{74}$$

The evaluation of the static term related to the internal force is of crucial importance to obtain the conservative character of the time integration scheme. The variation of the Green-Lagrange strain tensor is evaluated in the mid configuration, giving

$$G_{stat}\left(\Phi_n, \Phi_{n+1}, \delta\Phi\right) = \int_{M_0} \left(\mathbf{n} : \delta\varepsilon_{n+1/2} + \mathbf{q} : \delta\gamma_{n+1/2} + \mathbf{m} : \delta\kappa_{n+1/2}\right) dM_0 \tag{75}$$

The components of generalised stresses $\mathbf{n}$, $\mathbf{q}$, $\mathbf{m}$ are evaluated by means of a specific algorithmic form which is explained in the following. To ensure the properties of conservation of the time integration scheme, the generalised form of stress is computed by means of a particular algorithmic form. This makes possible to fulfil the Clausius-Duhem inequality. It can be shown that assuming a linear elastic constitutive model, the conservative algorithmic generalised components of stress are given by

$$n^{\alpha\beta} = \frac{1}{2} C^{\alpha\beta\gamma\delta} \left[\left(E^{(0)}_{\gamma\delta} \right)_{n+1} + \left(E^{(0)}_{\gamma\delta} \right)_{n} \right] \tag{76}$$

$$q^{\alpha 3} = \frac{1}{2} C^{\alpha 3\gamma 3} \left[\left(2E^{(0)}_{\gamma 3} \right)_{n+1} + \left(2E^{(0)}_{\gamma 3} \right)_{n} \right] \tag{77}$$

$$m^{\alpha\beta} = \frac{1}{2} C^{\alpha\beta\gamma\delta} \left[\left(E^{(1)}_{\gamma\delta} \right)_{n+1} + \left(E^{(1)}_{\gamma\delta} \right)_{n} \right] \tag{78}$$

In case of non-linear elastic or dissipative constitutive models, the algorithmic forms of the stress components are obtained as follows. The mean value theorem is applied to the variation of the Helmholtz free-energy function (28) in the generic time step

$$\Psi_{n+1} - \Psi_n = \left[\frac{\partial \Psi}{\partial \Gamma} \right]^T_{n+\beta} \cdot \left[\Gamma_{n+1} - \Gamma_n \right] \tag{79}$$

The comparison of the previous equation with the discrete (in time) form of the Clausius-Duhem inequality allows for defining the algorithmic forms of the generalised components of stress and dissipation

$$\left[\mathbf{n}, \mathbf{q}, \mathbf{m} \right]^T = \left[g \frac{\partial W}{\partial \Gamma} \right]_{n+\beta} \tag{80}$$

$$\Delta D^{int}_{n,n+1} = -\frac{1}{2} \left[W \frac{\partial g}{\partial \Gamma} \right]^T_{n+\beta} \cdot \left[\Gamma_{n+1} - \Gamma_n \right] \tag{81}$$

The method can be modified in order to ensure a quadratic convergence of the scheme with Δt. This procedure is based on the property of the function

$$\frac{1}{2}\left(\Psi_{n+\beta}-\Psi_{n+1-\beta}\right) \tag{82}$$

which enables to apply the mean value theorem as

$$\Psi_{n+1}-\Psi_n=\frac{1}{2}\left[\left(\frac{\partial\Psi}{\partial\Gamma}\right)_{n+\beta}+\left(\frac{\partial\Psi}{\partial\Gamma}\right)_{n+1-\beta}\right]^T\cdot\left[\Gamma_{n+1}-\Gamma_n\right] \tag{83}$$

This procedure leads to the alternative algorithmic forms

$$\left[\mathbf{n},\mathbf{q},\mathbf{m}\right]^T=\frac{1}{2}\left[\left(g\frac{\partial W}{\partial\Gamma}\right)_{n+\beta}+\left(g\frac{\partial W}{\partial\Gamma}\right)_{n+1-\beta}\right] \tag{84}$$

$$\Delta D^{int}_{n,n+1}=-\frac{1}{2}\left[\left(W\frac{\partial g}{\partial\Gamma}\right)_{n+\beta}+\left(W\frac{\partial g}{\partial\Gamma}\right)_{n+1-\beta}\right]^T\cdot\left[\Gamma_{n+1}-\Gamma_n\right] \tag{85}$$

Note that Eqs. (84), (85) and (86), (87) are equivalent as regards the properties of conservation in terms of energy. The scalar parameter β defines in practice the conservative configuration and it is deduced as the solution of the following non linear equation (with reference to Eq. (85))

$$h(\beta)=\Psi_{n+1}-\Psi_n-\frac{1}{2}\left[\left(\frac{\partial\Psi}{\partial\Gamma}\right)_{n+\beta}+\left(\frac{\partial\Psi}{\partial\Gamma}\right)_{n+1-\beta}\right]^T\cdot\left[\Gamma_{n+1}-\Gamma_n\right]=0 \tag{86}$$

The evaluation of the solution of Eq. (86) is performed at each time step at the Gauss point level. If the Helmholtz free-energy function is regular and if convexity is ensured, the solution can be obtained by means of the application of the Newton scheme. The procedure requires the derivation of the function h, hence the definition of the second order derivative of the Helmholtz free-energy function with respect to the strain. If elastic-damage behaviour is considered, we obtain

$$\begin{aligned}\frac{\partial^2\Psi(\Xi,\Gamma)}{\partial\Gamma\partial\Gamma}=g(\Xi)\left[\frac{\partial^2 W(\Gamma)}{\partial\Gamma\partial\Gamma}\right]+W(\Gamma)\left[\frac{\partial^2 g(\Xi)}{\partial\Gamma\partial\Gamma}\right]\\ +2\frac{g'(\Xi)}{\Xi}\left[\frac{\partial W(\Gamma)}{\partial\Gamma}\right]^T\left[\frac{\partial W(\Gamma)}{\partial\Gamma}\right]\end{aligned} \tag{87}$$

and the second order derivative of the damage function g is

$$\frac{\partial^2 g(\Xi)}{\partial\Gamma\partial\Gamma}=\left(\frac{g''}{\Xi}-\frac{g'}{\Xi^3}\right)\left[\frac{\partial W(\Gamma)}{\partial\Gamma}\right]^T\left[\frac{\partial W(\Gamma)}{\partial\Gamma}\right]+\frac{g'}{\Xi}\left[\frac{\partial W(\Gamma)}{\partial\Gamma}\right]^T\left[\frac{\partial W(\Gamma)}{\partial\Gamma}\right] \tag{88}$$

where the terms g' and g'' represent the derivative of the function g with respect to the equivalent strain Ξ. The lack of convexity sometimes requires the adoption of an alternative method for the solution of the equation instead of the Newton method. All the previous relations allow for writing the semi-discrete form of the balance

$$\frac{1}{\Delta t}\int_{M_0}\delta\Phi^T\begin{bmatrix}\mathbf{p}_{n+1}-\mathbf{p}_n & 0\\ 0 & \pi_{n+1}-\pi_n\end{bmatrix}dM_0+\int_{M_0}\mathbf{r}^T\left(\mathbf{B}_{n+1/2}\delta\Phi\right)dM_0 \tag{89}$$

The symbol $\mathbf{r}^T$ in the second term of the previous equation represents the conservative algorithmic form of generalised stress, given by relation (80) or (84). The evaluation of its components is made taking into account the values of the generalised stresses at time t_n and t_{n+1}. The latter are very simple to be found by means of the particular definition of the Helmholtz free-energy function, resulting in

$$\mathbf{n}_t = g\left(\Xi_t\right)C^{\mathbf{n}}\varepsilon_t \qquad (t=t_n,t_{n+1}) \tag{90}$$

$$\mathbf{q}_t = g\left(\Xi_t\right)C^{\mathbf{q}}\gamma_t \qquad (t=t_n,t_{n+1}) \tag{91}$$

$$\mathbf{m}_t = g\left(\Xi_t\right)C^{\mathbf{m}}\kappa_t \qquad (t=t_n,t_{n+1}) \tag{92}$$

Finally matrix $\mathbf{B}_{n+1/2}$ is the strain operator which allows for obtaining the variation of the strain components on the basis of the variation of configuration $\delta\Phi^T=[\delta\mathbf{u},\delta\mathbf{t}]$. The matrix $\mathbf{B}$ can be split pointing out membrane, transverse and bending components

$$\delta\varepsilon=\mathbf{B}^{\varepsilon}_{n+1/2}\delta\Phi \tag{93}$$

$$\delta\gamma=\mathbf{B}^{\gamma}_{n+1/2}\delta\Phi \tag{94}$$

$$\delta\kappa=\mathbf{B}^{\kappa}_{n+1/2}\delta\Phi \tag{95}$$

The configuration of the strain operator is simply given by a linear interpolation of the same operators evaluated at the time t_n and t_{n+1}

$$\mathbf{B}^{(\cdot)}_{n+1/2}=\frac{1}{2}\left[\mathbf{B}^{(\cdot)}_{n}+\mathbf{B}^{(\cdot)}_{n+1}\right] \tag{96}$$

More details about the terms of the strain operator $\mathbf{B}$ are given in the Appendix. Note how the semi-discrete weak form (89) is dependent on the unknown configuration Φ_{n+1} at the current time only.

Independent or simultaneous elastoplastic stress redistributions can be taken into account following an approach similar to the one followed in previous relations (87)-(89). In this case the dissipation should be divided into two parts, one controlled by the plastic function ϕ and one to the damage function g. The details will be reported in a later paper.

6 Space discretization

The basic aspect of the discretization in space is here explained. In what follows the indexes relating to time are omitted for sake of simplicity. Isoparametric four-node elements are adopted. The positions in the reference configuration and in the current configuration of a point belonging to the mid-plane of a generic element are given by

$$\mathbf{X}\left(\xi^1,\xi^2\right)\big|_\Omega = \sum_{I=1}^{4} N^I\left(\xi^1,\xi^2\right)\mathbf{X}_I \tag{97}$$

$$\mathbf{x}\left(\xi^1,\xi^2\right)\big|_\Omega = \sum_{I=1}^{4} N^I\left(\xi^1,\xi^2\right)\mathbf{x}_I \tag{98}$$

where $N^I\left(\xi^1,\xi^2\right)$ are the usual bilinear shape functions with $\left(\xi^1,\xi^2\right)\in[-1,+1]\times[-1,+1]$. In a similar way, the fields of the director of the shell and of the displacements, as well as of the linear and angular momentum, is given by the formulas

$$\mathbf{T}\left(\xi^1,\xi^2\right)\big|_\Omega = \sum_{I=1}^{4} N^I\left(\xi^1,\xi^2\right)\mathbf{T}_I \tag{99}$$

$$\mathbf{t}\left(\xi^1,\xi^2\right)\big|_\Omega = \sum_{I=1}^{4} N^I\left(\xi^1,\xi^2\right)\mathbf{t}_I \tag{100}$$

In order to avoid a possible 'locking' given by the thin thickness of the shell elements, the ANS method is here adopted. The field of transverse shear strains is assumed as linearly varying from the opposite edges of a generic element. In the mid-point of every edge the shear strain components are given by

$$2\bar{E}^{(0)}_{13} = \frac{1}{2}\left(1-\xi^2\right)2E^{(0)A}_{13} + \frac{1}{2}\left(1+\xi^2\right)2E^{(0)C}_{13} \tag{101}$$

$$2\bar{E}^{(0)}_{23} = \frac{1}{2}\left(1-\xi^1\right)2E^{(0)D}_{23} + \frac{1}{2}\left(1+\xi^2\right)2E^{(0)B}_{23} \tag{102}$$

The points of the mid surface $\mathbf{x}^L$ with $L=A,B,C,D$ are given by the following expressions

$$\mathbf{x}^L = \frac{1}{2}\mathbf{x}\left(\xi^1_M,\xi^2_M\right) + \frac{1}{2}\mathbf{x}\left(\xi^1_N,\xi^2_N\right) \tag{103}$$

being $(L,M,N)\in\{(A,1,2),(B,2,3),(C,3,4),(D,1,4)\}$. Finally, the interpolations of the necessary terms of the discretization in space of the semi-discrete weak form are given by

$$\delta\mathbf{u}|_\Omega = \sum_{I=1}^{4} N^I\delta\mathbf{u}_I, \quad \delta\mathbf{t}|_\Omega = \sum_{I=1}^{4} N^I\delta\mathbf{t}_I \tag{104}$$

$$\left.\frac{\partial \mathbf{u}}{\partial \xi^\alpha}\right|_\Omega = \sum_{I=1}^{4} \frac{\partial N^I}{\partial \xi^\alpha}\mathbf{u}_I, \quad \left.\frac{\partial \mathbf{t}}{\partial \xi^\alpha}\right|_\Omega = \sum_{I=1}^{4} \frac{\partial N^I}{\partial \xi^\alpha}\mathbf{t}_I \tag{105}$$

$$\left.\frac{\partial \delta\mathbf{u}}{\partial \xi^\alpha}\right|_\Omega = \sum_{I=1}^{4} \frac{\partial N^I}{\partial \xi^\alpha}\delta\mathbf{u}_I, \quad \left.\frac{\partial \delta\mathbf{t}}{\partial \xi^\alpha}\right|_\Omega = \sum_{I=1}^{4} \frac{\partial N^I}{\partial \xi^\alpha}\delta\mathbf{t}_I \tag{106}$$

With the previous relations at hand, the full discrete weak form of the balance of momentum can be obtained by Eq. (89).

7 Linearisation aspects

The full discrete form of the weak form of the balance of momentum consists of a system of equations which has nodal displacements and rotations (evaluated at the current time t_{n+1}) as unknown terms. The solution of the system is found by means of the application of the Newton-Raphson method. Hence the directional derivative

$$DG_{din}\left(\dot{\Phi}_n, \Phi_n, \Phi_{n+1}^{(i)}, \delta\Phi\right) \cdot \Delta\Phi_{n+1}^{(i)} = -G_{din}^{(i)} \tag{107}$$

must be evaluated in order to improve the trial solution until a specified norm results below the specified tolerance. The derivative leads to three terms, usually known as inertial, material and geometric, indicated by D_D, D_M and D_G respectively.

$$\begin{aligned} &D_D G_{din} \cdot \Delta\Phi_{n+1} \\ &\quad = \bigcup_{e=1}^{Nelem} \int_{\Omega_e} \left[\frac{2A_{\rho_0}}{(\Delta t)^2}\Delta\mathbf{u}_{n+1} \cdot \delta\mathbf{u} \frac{2I_{\rho_0}}{(\Delta t)^2}\Delta\mathbf{t}_{n+1} \cdot \delta\mathbf{t} + \frac{1}{\Delta t}\left(\pi_{n+1} - \pi_n\right) \cdot \Delta\left(\delta\mathbf{t}\right) \right] d\Omega_e, \end{aligned} \tag{108}$$

$$\begin{aligned} D_G G_{din} \cdot \Delta\Phi_{n+1} &= \bigcup_{e=1}^{Nelem} \int_{\Omega_e} \mathbf{r} \cdot \left[D\left(\delta\mathbf{E}\right) \cdot \Delta\Phi_{n+1}\right] d\Omega_e \\ &= \bigcup_{e=1}^{Nelem} \int_{\Omega_e} \mathbf{r} \cdot \left\{ \frac{1}{2}\left[D\left(\mathbf{B}_{n+1}\right) \cdot \Delta\Phi_{n+1}\right] \delta\Phi + \mathbf{B}_{n+1/2} D\left(\delta\Phi\right) \cdot \Delta\Phi_{n+1} \right\} d\Omega_e \end{aligned} \tag{109}$$

$$D_M G_{din} \cdot \Delta\Phi_{n+1} = \bigcup_{e=1}^{Nelem} \int_{\Omega_e} \left(\mathbf{B}_{n+1/2}\delta\Phi\right) \cdot \left(D\mathbf{r} \cdot \Delta\Phi_{n+1}\right) d\Omega_e \tag{110}$$

On the basis of the Helmholtz free-energy function defined in section 3 the derivative of the internal forces in the previous term gives the following expression

$$
\begin{aligned}
D\mathbf{r} = & \frac{1}{2}\left[\beta_0 g\left(\Xi_{n+\beta_0}\right) + (1-\beta_0)\, g\left(\Xi_{n+1-\beta_0}\right)\right] C\mathbf{B}_{n+1}\Delta\Phi_{n+1} \\
& + \frac{1}{2}\beta_0 \frac{\dot{g}\left(\Xi_{n+\beta_0}\right)}{\Xi_{n+\beta_0}} \left[\frac{\partial W(\Gamma)}{\partial \Gamma}\right]^T_{n+\beta_0} \left[\frac{\partial W(\Gamma)}{\partial \Gamma}\right]_{n+\beta_0} \cdot \mathbf{B}_{n+1}\Delta\Phi_{n+1} \\
& + \frac{1}{2}(1-\beta_0) \frac{\dot{g}\left(\Xi_{n+1-\beta_0}\right)}{\Xi_{n+1-\beta_0}} \cdot \left[\frac{\partial W(\Gamma)}{\partial \Gamma}\right]^T_{n+1-\beta_0} \left[\frac{\partial W(\Gamma)}{\partial \Gamma}\right]_{n+1-\beta_0} \mathbf{B}_{n+1}\Delta\Phi_{n+1} \quad (111)
\end{aligned}
$$

where the coefficient β_0 is the value ensuring the conservative character of the algorithmic internal stresses, as previously explained. Similar developments should be considered in case of elastoplastic behaviour, as it will be shown in a later paper.

8 Examples

The following examples show the main properties of the algorithm in terms of fulfillment of the balance laws, both as regards momentum and energy of the system. Attention is also focused on the convergence property of the scheme, resulting second order by a consistent linearization of the vector of internal forces.

8.1 Dynamics of a damaged shell

In this example the comparison between hemispherical shells with a linear elastic and an elastic-damaged constitutive laws is presented. The material parameters taken into account are: Young's modulus E = 203 GPa and Poisson's ratio $\nu = 0.3$, energy at the beginning of damage process $\tau = 3$ and at the final material collapse $\tau = 75$ (corresponding to a strain equal to 5% and 125%, respectively, in uniaxial traction and compression). As far as the geometrical characteristics are concerned, a diameter equal to 10 m has been assumed and a thickness/diameter ratio of 1/100. The numerical experiment has been carried out in displacement control (due to the softening behaviour in the damaged range), imposing a vertical displacement to the upper point of the shell up to the material collapse in the damaged case.

It can be noticed that the mechanism of shell deformation is twofold (Figure 2 evidences the different deformed shapes in the damaged and elastic configurations). One is related to the high membrane stresses in the zone close to the apex, the other is due to the bending stresses in the zone where the maximum curvature is attained. The results are summarized into two diagrams. The first one (Figure 3) represents the reaction at the apex (where the displacement has been imposed) vs. the apex vertical displacement. The loading phase and elastic unloading (in pink)

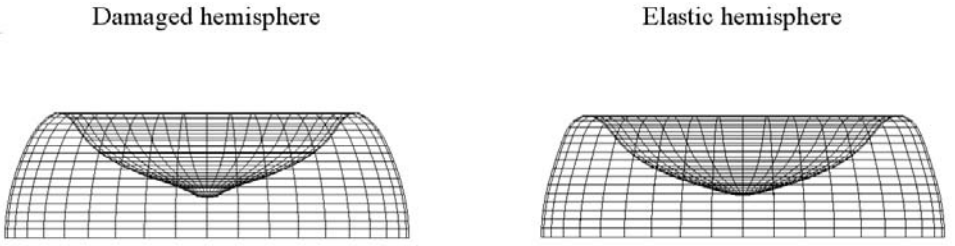

Figure 2: Comparison between deformed shapes of damaged and elastic hemispheres.

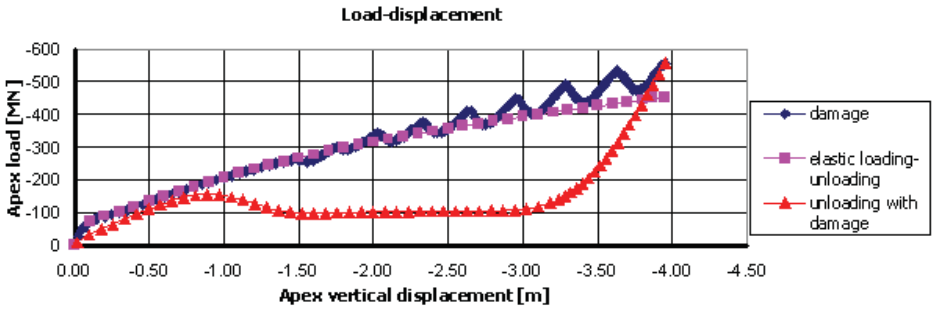

Figure 3: Reaction vs. displacements at the apex of the hemisphere where a vertical displacement is imposed.

are evidenced, while the blue and red lines represent the loading and unloading phases of the damaged material, respectively.

The finite strain model used for the shell allowed to discover that the damaged hemisphere is more rigid than the elastic one. The oscillations in the loading phase of the hemispherical damaged shell are due to the specific mechanism of deformation: the first separation between the curve representing the damaged material and that of the elastic one appears when the limit bending stress is attained along a ring of elements at about half the height of the hemisphere. Due to the softening material behaviour (a descending branch in the reaction-displacements diagram can be seen, Figure 3) a complete rotation of the elements belonging to the ring can be observed until they are no more subjected to bending but to a membrane action and hence an increase in stiffness can be seen (the slope of the diagram is again positive).

This “saw” effect is clearly shown in Figure 3. The decrease in the lever effect due to the above mechanism in the damaged hemisphere results in a more rigid be-

haviour of the shell, up to the final collapse. Such oscillations can be circumvented by a nonlocal damage approach still to be implemented. For a better understanding of this behaviour, a second diagram has been produced (Figure 4), where the polar mapping of damage level is represented: the main damage effect is concentrated at the top and half height of the hemispherical shell.

Additionally, Figure 5 depicts the membrane and bending stresses for both the damaged and elastic hemisphere.

8.2 Dynamic stability of an elastoplastic shell

A second example concerns the case of an elastoplastic instability phenomenon found again in an hemispherical shell subjected to a concentrated load at the top. The adopted material is supposed to be steel (Young's modulus E = 203 GPa and Poisson's ratio $\nu = 0.3$, yield limit $k_0 = 1680$ MPa, corresponding to a 0.8% deformation and isotropic hardening modulus k' = 250 MPa). The kinematic hardening is set equal to zero, in this case, for a clearer interpretation of the numerical results. The instability phenomenon was discovered to be dependent on the adopted FE mesh and on the applied loading speed. Deformed shapes with three, four and six waves have been found. The numerical experiment has been carried out in displacement control during loading and in force control during recovery. In the following only the experiment corresponding to the three waves case is shown. The contour maps of shear and bending stress resultants acting on the faces of the elements are shown in Figure 6, for both the plastic and elastic hemisphere. The shear stress, zero in the elastic case, assumes a primary role in the elastoplastic one.

As in the previous example, a diagram showing the reaction at the hemisphere apex (where a vertical displacement is imposed) vs. the apex vertical displacement is reported (Figure 7). As in the previous case, due to the different deformation mechanisms involved, the structure stressed in the plastic range is more rigid than the one deformed in the elastic domain. At unloading, a straight line can be seen, demonstrating that the recovery happens in a purely elastic stage and in membrane regime. Moreover, the irreversible plastic strains are mainly of membrane type.

As far as the instability mechanism is concerned, a change in the deformed shape, from an axial-symmetric one to a shape with three or four waves, has been observed, linked to an increasing load and to the imposed boundary conditions. In the following an explanation of the phenomenon is given. First of all, it should be noticed that the finite strain effects in the elastoplastic range leads the structure to withstand to the applied load in a completely different way compared to the elastic case.

When the elastic limit is attained, the bending along a ring of elements allows for

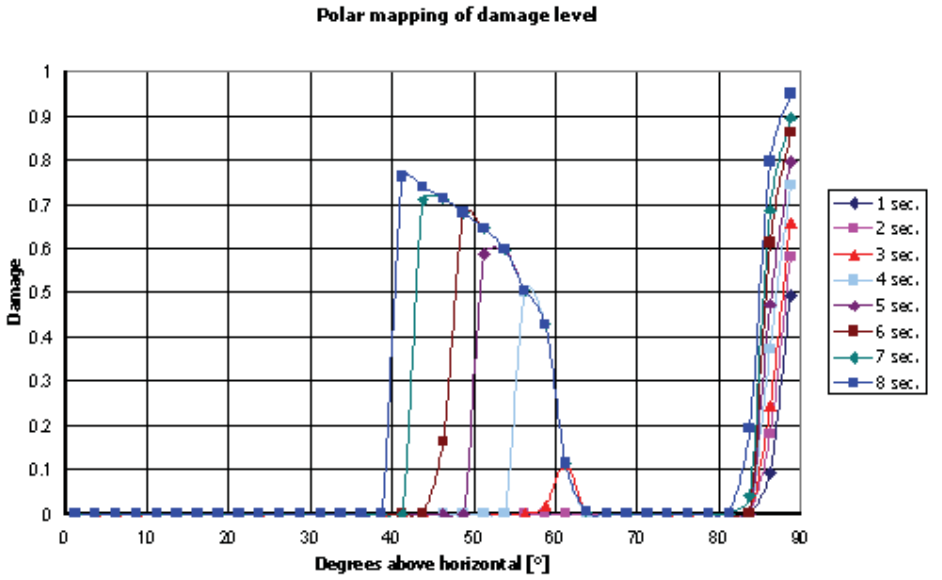

Figure 4: Damage vs. hemisphere latitude (from equator) at different time stations.

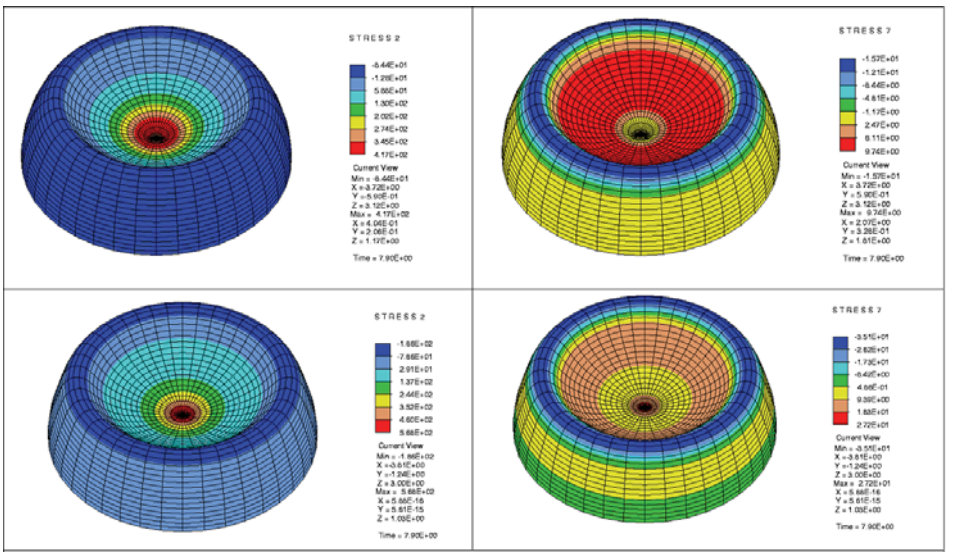

Figure 5: Membrane (left) and bending (right) stresses for the damaged (top) and elastic (bottom) hemisphere.

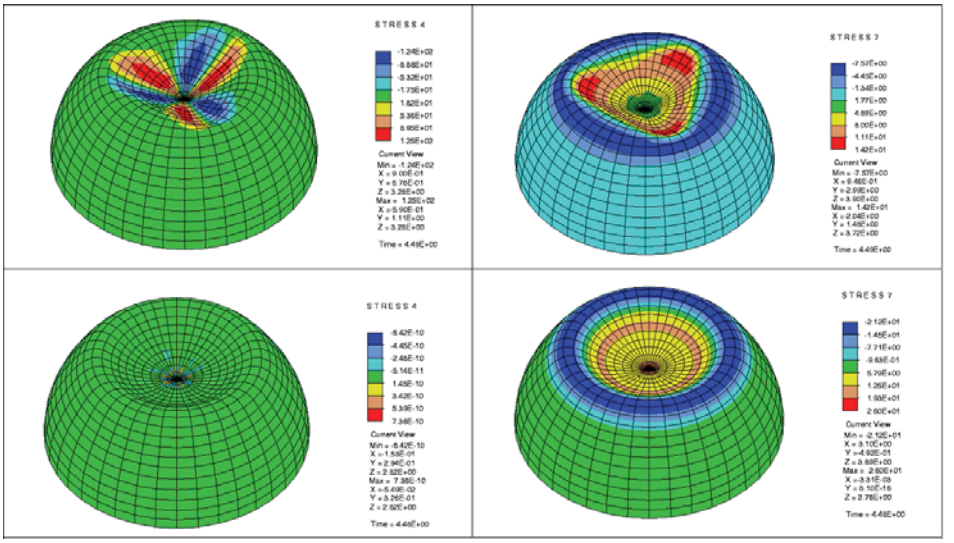

Figure 6: Shear (left) and bending (right) stresses for the plastic (top) and elastic (bottom) hemisphere.

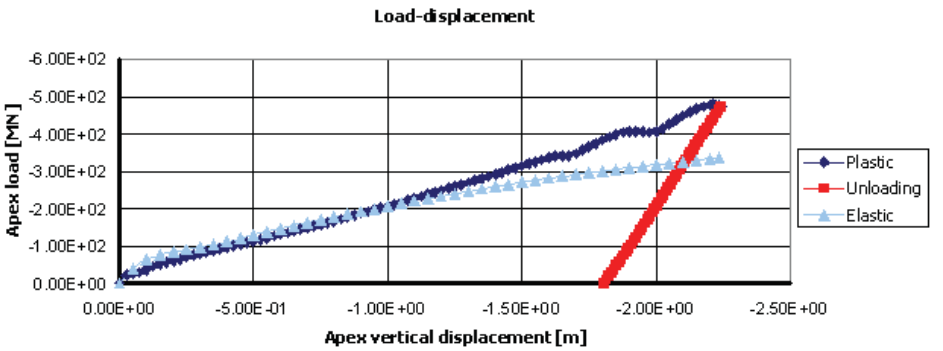

Figure 7: Reaction vs. displacements at the apex of the hemisphere where a vertical displacement is imposed.

the formation of plastic hinges, causing the top elements to displace inner wards to the shell. After experiencing such a rotation, the element is no more stressed by bending, being the dominant action represented by the membrane one. The structure can be divided into two zones: the central one, highly stressed in traction and where plastic deformations occur, and the surrounding zone, still in the elastic range, where the stress state is mainly of membrane type. On the other hand, in

the elastic case, the structure assumes a smoother curvature with a more balanced distribution of membrane and bending stresses. For comparison purposes, the instability modes of a ring subject to radial forces have been found and the critical load determined. In this case a commercial FE code has been used [Straus7 (2004)].

The second and third buckling shapes in Figure 8 correspond to the deformed configuration of the hemispherical shell in the two previously recalled instability cases (they depend on the chosen boundary conditions). To confirm the above behaviour, the case of a portion of a cone has also been analysed, applying an inner wards radial load, as shown in Figure 9a.

Even in this situation very similar results to the case of the hemispherical shell have been obtained, with the exception of the first shape which is elliptical (Figures 10b,c,d). At the end, the numerical experiment has been carried out directly on the hemispherical shell.

The deformed shape immediately before the instability phenomenon has been assumed as the initial deformed configuration and the central elements at the top have been excluded. The hemisphere has been fully hinged at the equatorial line (vertical supports along the line and free rotations around it) as in the experiments carried out with our approach. Hence the boundary conditions produced the jump of the first buckling shape. The results are shown in Figure 10.

The specific adopted boundary conditions resulted in an inversion of the first two buckling deformed shapes, also taking into account that the load multipliers in the two cases are very close (they differ by only a 6%). Finally, a vertical buckling load of 300000 KN has been estimated. The deformed shape of the central part of the hemisphere has been approximated by a cone and a pure membrane stress state has been applied. As a consequence, the ratio between the vertical and the horizontal components of the load resulted equal to 0.36. Finally, the plastic moment acting in the inner side of the elements has been estimated. The found instability deformed shapes are again in agreement with the previous results. The three-waves deformed shape appeared for a loading multiplier higher than in the case of the four-waves shape, but the multipliers are again very close (the difference is now 5.6 %).

9 Conclusions

The proposed work is a contribution to the actual development of fully nonlinear shell solutions using FEM. In the chosen approach finite rotations, displacements and strains are incorporated. Nonlinear constitutive laws like hyperelastic-damaged and elastoplasticity are also included. Tangent stiffness matrices ensures quadratic convergence and hence fast, accurate and robust solution. Post-buckling behavior, elastoplastic and hyperelastic-damaged solution are compared for different geo-

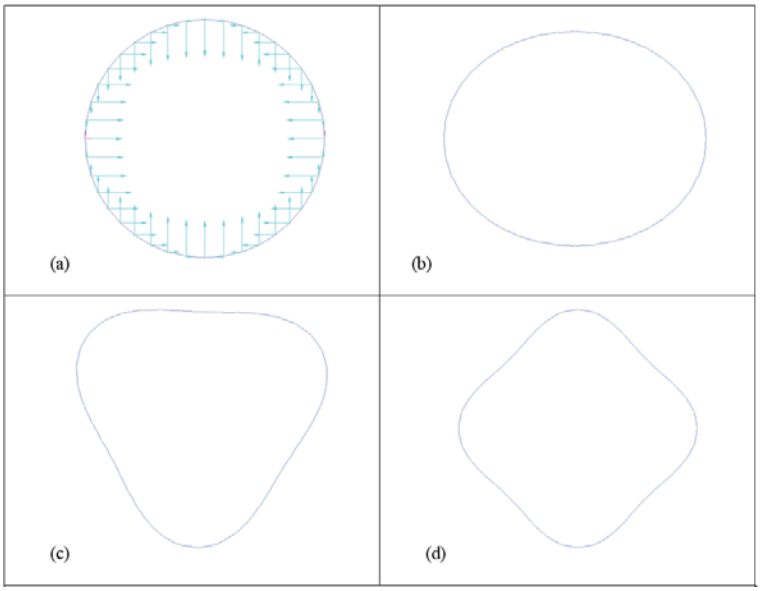

Figure 8: Circular ring subject to radial load (a); 1^{st} buckling shape (b), 2^{nd} shape (c), 3^{rd} shape (d).

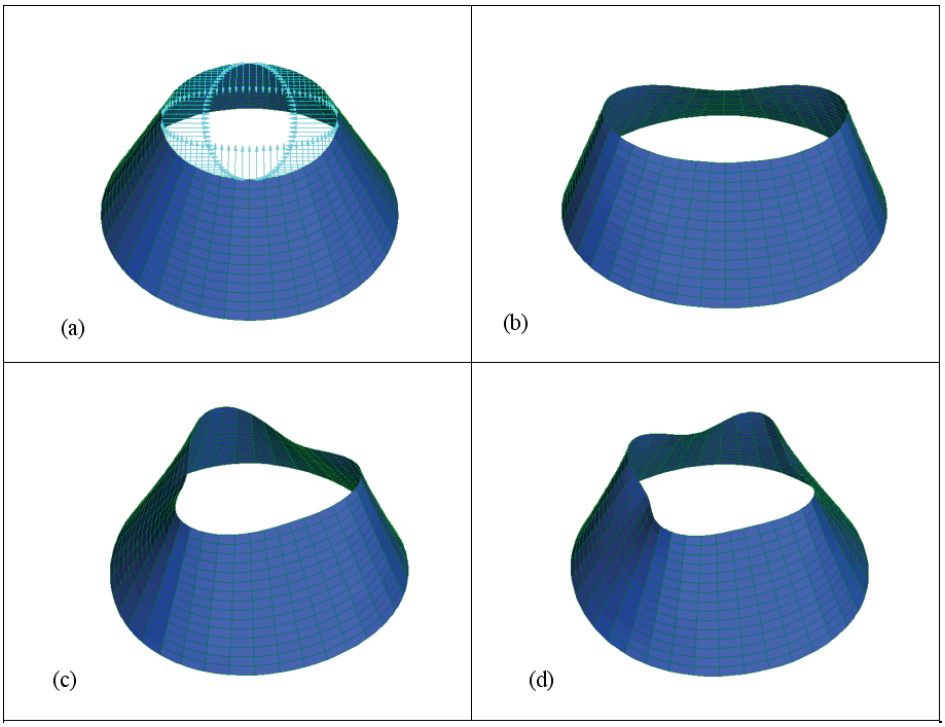

Figure 9: Portion of a cone subject to radial load (a); 1^{st} buckling shape (b), 2^{nd} shape (c), 3^{rd} shape (d).

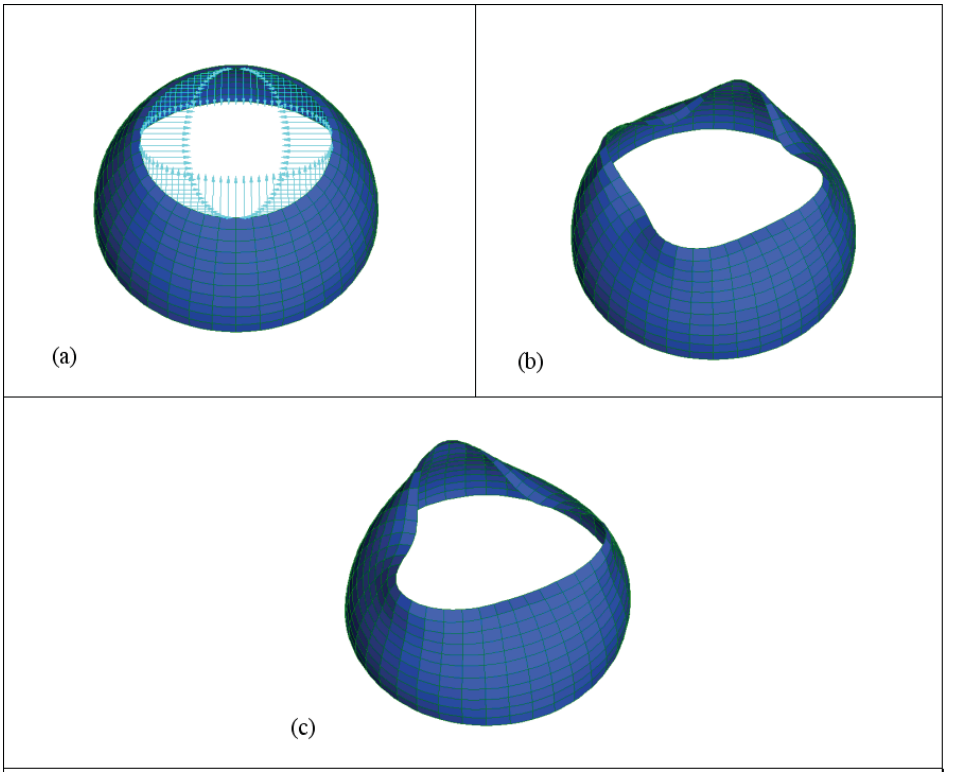

Figure 10: Portion of an hemisphere subject to radial load (a); 1^{st} buckling shape (b), 2^{nd} shape (c).

metrically exactly described shapes. This paper can be useful for comparisons with solutions presented in several cited papers in the field, where alternative approaches to FEM were mainly used, like MLPG and BEM. Useful comparison can be made in terms of solution speed, incorporation of concurrent nonlinear material and geometrical effects, number of equation in the resolving matrices, etc.

More in detail, a non-linear dynamic analysis of thin shells has been presented here. Among the features of this shell element, the fulfilment of an energy-momentum method has been recalled which, together with a consistent numerical formulation, allowing for a fast and accurate time integration of the shell. The adopted constitutive relationships incorporate hyperelasticity, scalar elastic-damage mode and an elastoplastic one including isotropic/kinematic hardening. The conservative characteristics of the time integration algorithm are still valid if applied to a structural system with internal dissipation. The stability of the time integration scheme

arising from the particular choice of algorithmic forms of the stresses and internal dissipation must be intended as the fulfilment of the discrete form in time of the Clausius-Duhem inequality. The shell model allows to describe the dynamics of real structures made of materials with internal dissipation and undergoing large displacements, rotations and moderately large deformations.

Acknowledgement: The authors gratefully thank Dr. Carlo Janna for the help given during the preparation of the numerical examples.

References

Areias, P.M.A.; Song, J.-H.; Belytschko, T. (2005): A finite-strain quadrilateral shell element based on discrete Kirchhoff–Love constraints, *Int. J. Num. Meth. Engrg*., vol. 64, pp. 1166-1206.

Argyris, J.H.; Papadrakakis, M.; Karapitta, L. (2002): Elasto-plastic analysis of shells with the triangular element TRIC, *Comp. Meth. Appl. Mech. Engrg*., vol. 191, pp. 3613-3636.

Baiz, P.M.; Aliabadi, M.H. (2006): Linear buckling analysis of shear deformable shallow shells by the Boundary Domain Element Method, *CMES: Computer Modeling in Engineering & Sciences*, vol. 13(1), pp.19-34.

Başar, Y.; Kintzel, O. (2003): Finite rotations and large strains in finite element shell analysis, *CMES: Computer Modeling in Engineering & Sciences*, vol. 4(2), pp. 217-30.

Brank, B.; Briseghella, L.; Tonello, N.; Damjanic, F. (1998): On non-linear dynamics of shells: Implementation of energy-momentum conserving algorithm for a finite rotation shell model, *Int. J. Num. Methods Engrg*., vol.42, pp. 409-442.

Brank, B.; Mamouri, S.; Ibrahimbegoviæ, A. (2005): Constrained finite rotations in dynamics of shells and Newmark implicit time-stepping schemes, *Engrg. Comp*., vol. 22(5-6), pp. 505-535.

Briseghella, L.; Corazzin, L.; Majorana, C.E.; Pavan, P. (1997): Conservative algorithms for time integration of elastodynamics response in finite strains, *Int. J. Engrg. Model*., vol. 10, pp. 1-5.

Briseghella, L.; Majorana, C.E.; Pavan, P. (1998): Exact evaluation of dissipation for elastic-damage model dynamics, *Comp. Meth. Appl. Mech. Engrg*., vol. 157, pp. 11-18.

Briseghella, L.; Majorana, C.E.; Pavan, P. (2000): Extension of the energy-momentum method to non-linear dynamics of elasto-damaged thin shells, in: Proc. *ICES2K Conf*., Los Angeles, USA, Aug. 20-25.

Briseghella, L.; Majorana, C.E.; Pavan, P. (2003): A conservative time integration scheme for dynamics of elasto-damaged thin shells, *CMES: Computer Modeling in Engineering & Sciences*., vol. 4(2), pp. 273-286.

Briseghella, L.; Majorana, C.E.; Pellegrino, C. (1998): Dynamic Stability of Elastic Structures: a Finite Element Approach, *Comp. Struct*., vol. 69, pp. 11-25.

Briseghella, L.; Majorana, C.E.; Pellegrino, C. (1999): Conservation of angular momentum and energy in the integration of non-linear dynamic equations, *Comp. Meth. Appl. Mech. Engrg*., vol. 179, pp. 247-263.

Chui, X.Y.; Liu, G.R.; Li, G.Y.; Zhao, X.; Nguyen, T.T.; Sun, G.Y. (2008): A smoothed Finite Element Method (SFEM) for linear and geometrically nonlinear analysis of plates and shells, *CMES: Computer Modeling in Engineering & Sciences*, vol. 28(2), pp.109-125.

Dvorkin, E.N.; Bathe, K.J. (1984): A continuum mechanics based four-node shell element for general non-linear analysis, *Engrg. Comp*., vol. 1, pp. 77-88.

Gawin, D.; Majorana, C.E.; Schrefler B.A. (1999): Numerical analysis of hygrothermal behaviour and damage of concrete at high temperature, *Mech. Cohe. Frict. Mat*., vol. 4, pp. 37-74.

Janna, C.; Majorana, C.E.; Zavarise, G. (2004): Elastoplastic and damage behaviour of shells subject to finite displacements and rotations, in: Proc. *GIMC-AIMETA, Italian Group of Comp. Mech. – Italian Ass. of Theor. and Appl. Mech.*, Genova, June 21-23. In Italian.

Jarak, T.; Soric, J.; Hoster, J. (2007): Analysis of shell deformation responses by the Meshless Local Petrov-Galerkin (MLPG) approach, *CMES: Computer Modeling in Engineering & Sciences*, vol. 18(3), pp.235-246.

Kulikov, G.M.; Plotnikova, S.V. (2006): Non-linear strain–displacement equations exactly representing large rigid-body motions. Part II - Enhanced finite element technique, *Comp. Meth. Appl. Mech. Engrg*., vol. 195, pp. 2209-2230.

Kulikov, G.M.; Plotnikova, S.V. (2008): Finite rotation geometrically exact four-node solid-shell-element with seven displacement degrees of freedom, *CMES: Computer Modeling in Engineering & Sciences*, vol. 28(1), pp.15-38.

Majorana, C.E.; Bressanin, S.; Rigo Serra, J.; Zavarise, G. (2002): Computational analysis of contact mechanics in shells undergoing large displacements and rotations, in: Proc. *GIMC 2002, 3rd Joint Conf. of Italian Group of Comp. Mech. and Ibero-Latin American Ass. of Comp. Methods in Engrg*., Giulianova, 24-26 June. In Italian.

Majorana, C.E.; Pellegrino, C. (1999): Dynamic stability of beams with finite displacements and rotations, *Engrg. Comp*., vol. 16(6), pp. 639-658.

Providakis, C.P. (2007): The effect of internal support conditions to the elasto-plastic transient response of Reissner-Mindlin plates, *CMES: Computer Modeling in Engineering & Sciences*, vol. 18(3), pp.247-258.

Salomoni, V.A.; Majorana, C.E.; Giannuzzi, G.M.; Miliozzi, A. (2008): Thermal-fluid flow within innovative heat storage concrete systems for solar power plants, *Int. J. Num. Meth. Heat Fluid Flow* (Special Issue). In press.

Salomoni, V.A.; Mazzucco, G.; Majorana, C.E. (2007): Mechanical and durability behaviour of growing concrete structures, *Engrg. Comp*., vol. 24(5), pp. 536-561.

Sansour, C.; Wagner, W.; Wriggers, P.; Sansour, J. (2002): An energy–momentum integration scheme and enhanced strain finite elements for the non-linear dynamics of shells, *Int. J. Non-Linear Mech*., vol. 37, pp. 951–966.

Sharnappa, Ganesan, N.; Raju Sethuraman (2007): Buckling and free vibrations of sandwich general shells of revolution with composite facings and viscoelastic core under thermal environment using Semi-analytical method, *CMES: Computer Modeling in Engineering & Sciences*, vol. 18(2), pp.121-144.

Simo, J.C. (1987): On a fully three-dimensional finite-strain viscoelastic damage model: formulation and computational aspects, *Comp. Methods App. Mech. Engrg*., vol. 60, pp. 153-173.

Simo, J.C., Rifai, M.S.; Fox, D.D. (1992): On stress resultant geometrically exact shell model - Conserving algorithms for non-linear dynamics, *Int. J. Num. Meth. Engrg*., vol. 34, pp. 117-164.

Simo, J.C.; Kennedy, J.G.; Govindjee, S. (1988): Non-smooth multisurface plasticity and viscoplasticity. Loading/unloading conditions and numerical algorithms, *Int. J. Num. Meth. Engrg*., vol. 26, pp. 2161-2185.

Simo, J.C.; Tarnow, N. (1992): The discrete energy-momentum method - Conserving algorithms for nonlinear elastodynamics, *Z. Agnew. Math. Phys*., vol. 43, pp. 757-792.

Simo, J.C.; Tarnow, N.; Doblare, M. (1995): On non-linear dynamics of three-dimensional rods: exact energy and momentum conserving algorithms, *Int. J. Num. Meth. Engrg*., vol. 38, pp. 1431-1474.

Simo, J.C.; Wong, K.K. (1991): Unconditionally stable algorithms for rigid body dynamics that exactly preserve energy and momentum, *Int. J. Num. Meth. Engrg*., vol. 31, pp. 19-52.

Sladek, J.; Sladek, V.; Wen, P.H.; Aliabadi, M.H. (2006): Meshless local Petrov-Galerkiin (MLPG) method for shear deformable shells analysis, *CMES: Computer Modeling in Engineering & Sciences*, vol. 13(2), pp.103-117.

Straus7 (2004): Theoretical Manual. Strand7 Pty Ltd.

Suetake, Y.; Iura, M.; Atluri, S.N. (2003): Variational formulation and symmetric tangent operator for shells with finite rotation field, *CMES: Computer Modeling in Engineering & Sciences*, vol. 4(2), pp. 329-336.

Suetake, Y. (2006): Plate bending analysis by using a modified plate theory, *CMES: Computer Modeling in Engineering & Sciences*, vol. 11(3), pp.103-110.

Tonkovic, Z.; Soric, J.; Skozrit, I. (2008): On numerical modeling of cyclic elastoplastic response of shells structures", *CMES: Computer Modeling in Engineering & Sciences*, vol. 26(2), pp.75-90.

Wen, P.H. and Hon, Y.C. (2007): Geometrically nonlinear analysis of Reissner-Mindlin plate by meshless computation, *CMES: Computer Modeling in Engineering & Sciences*, vol. 21(3), pp.177-191.

Appendix

The terms of the matrix of the stored energy function (27) are given by

$$C^n = \frac{EH}{1-\nu^2}\bar{C} \quad C^q = \chi GH\bar{\bar{C}} \quad C^m = \frac{EH^3}{12\,(1-\nu^2)}\bar{C} \tag{A.1}$$

where the matrix $\bar{\bar{C}}$ and $\bar{C}$ are given respectively by

$$\bar{\bar{C}} = \begin{bmatrix} A^{11} & A^{12} \\ \text{symm.} & A^{22} \end{bmatrix} \tag{A.2}$$

and

$$\bar{C} = \begin{bmatrix} A^{11}A^{11} & \nu A^{22}A^{11} + (1-\nu)A^{12}A^{12} & A^{11}A^{12} \\ & A^{22}A^{22} & A^{22}A^{12} \\ \text{symm.} & & \frac{1-\nu}{2}A^{11}A^{12} + \frac{1+\nu}{2}A^{12}A^{12} \end{bmatrix} \tag{A.3}$$

Here H is the thickness of the shell. The coefficients E, G, ν, are the Young's modulus, the shear modulus and the Poisson's ratio. Finally χ represents the shear factor.

The expressions of the strain operators used in (93), (94) and (95) are given by

$$\mathbf{B}_n^{\varepsilon} = \begin{bmatrix} \frac{\partial \mathbf{x}}{\partial \xi^1}^T \frac{\partial}{\partial \xi^1} & \mathbf{0} \\ \frac{\partial \mathbf{x}}{\partial \xi^1}^T \frac{\partial}{\partial \xi^1} & \mathbf{0} \\ \frac{\partial \mathbf{x}}{\partial \xi^1}^T \frac{\partial}{\partial \xi^2} + \frac{\partial \mathbf{x}}{\partial \xi^2}^T \frac{\partial}{\partial \xi^1} & \mathbf{0} \end{bmatrix}_n \tag{A.4}$$

$$\mathbf{B}_n^{\gamma} = \begin{bmatrix} \mathbf{t}^T \frac{\partial}{\partial \xi^1} \frac{\partial \mathbf{x}}{\partial \xi^1}^T \\ \mathbf{t}^T \frac{\partial}{\partial \xi^2} \frac{\partial \mathbf{x}}{\partial \xi^2}^T \end{bmatrix}_n \tag{A.5}$$

$$\mathbf{B}_n^{\kappa} = \begin{bmatrix} \frac{\partial \mathbf{t}}{\partial \xi^1}^T \frac{\partial}{\partial \xi^1} & \frac{\partial \mathbf{x}}{\partial \xi^1}^T \frac{\partial}{\partial \xi^1} \\ \frac{\partial \mathbf{x}}{\partial \xi^2}^T \frac{\partial}{\partial \xi^2} & \frac{\partial \mathbf{x}}{\partial \xi^2}^T \frac{\partial}{\partial \xi^2} \\ \frac{\partial \mathbf{t}}{\partial \xi^1}^T \frac{\partial}{\partial \xi^2} + \frac{\partial \mathbf{t}}{\partial \xi^2}^T \frac{\partial}{\partial \xi^1} & \frac{\partial \mathbf{x}}{\partial \xi^1}^T \frac{\partial}{\partial \xi^2} + \frac{\partial \mathbf{x}}{\partial \xi^2}^T \frac{\partial}{\partial \xi^1} \end{bmatrix}_n \tag{A.6}$$